Journal of Applied Polymer Science

Physical and Mechanical Properties of the Fully Interconnected Chitosan Ice-Templated Scaffolds

Masoud Pourhaghgouy, Ali Zamanian
Department of Nanotechnology and Advanced Materials, Materials and Energy Research Center, P. O. Box 13145-1659, Karaj, Iran
Correspondence to: A. Zamanian (E-mail: a-zamanian@merc.ac.ir)

ABSTRACT: Porous chitosan scaffolds were prepared with a freeze-casting technique with different concentrations, 1.5 and 3 wt %, and also different cooling rates, 1 and 4°C/min. The pore morphology, porosity, pore size, mechanical properties, and water absorption characteristics of the scaffolds were studied. Scanning electron microscopy images showed that the freeze-cast scaffolds were fully interconnected because of the existence of pores on the chitosan walls in addition to many unidirectionally elongated pores. Increases in the chitosan concentration and freezing rate led to elevations in the thickness of the chitosan walls and reductions in the pores size, respectively. These two results led to the enhancement of the compressive strength from 34 to 110 kPa for the scaffolds that had 96–98% porosity. Also, augmentation of the chitosan concentration and decreases in the freezing rate led to the reduction of the number of pores on the chitosan walls. Furthermore, the volume of water absorption increased with a reduction in the chitosan concentration and cooling rate from 690 to 1020%. © 2014 Wiley Periodicals, Inc. J. Appl. Polym. Sci. **2015**, *132*, 41476.

KEYWORDS: mechanical properties; morphology; polysaccharides; porous materials; properties and characterization

Received 30 June 2014; accepted 2 September 2014
DOI: 10.1002/app.41476

INTRODUCTION

The wide applications of porous materials in catalyst carriers, ceramic filters, sensors, porous electrodes, thermal barriers, biomaterials, and so on have made this type of material very attractive for researchers.[1–3] In the case of biomaterials applications, there are lots of important points that should be noted in the application of porous scaffolds in tissue engineering. As the beginning phase, to guarantee the supply of cells with nutrients and to ease tissue integration and vascularization, the existence of interconnecting pores has a great importance. Also, the size and morphology of the pores are essential traits for cell penetration and tissue regeneration.[4] The mechanical properties of the scaffolds should have similar values as in natural tissues. The biocompatibility and biodegradability of the scaffold materials are also very important.[5] Various fabrication methods of porous scaffolds have been used, including solvent casting,[6] gel casting,[7] gas foaming,[8] phase separation,[9] electrospinning,[10] freeze drying,[11] and freeze casting.[12] Freeze casting, or ice templating, which has gained a great deal of attention over the past few years, is a simple technique for producing porous materials, including not only ceramics but also polymers and metals.[13–15] This method has many benefits, such as the adaptability of the process, a slight contraction process, controlled pore size variety, a high strength, and its environmentally friendliness.[16] A porous structure containing unidirectional channels is generated as a result of the unidirectional freezing of a liquid suspension (aqueous or not) followed by the sublimation of the solidified solvent under low pressure, and the pores are located in the same position of the solvent crystals.[12,17] Various liquids can be used as solvents, but the most common is water for plenty of reasons, including its ease of use, good environmental features, the unique morphologies of ice crystals, and its compatibility with functional additives.[18] The ejection of particles from the growing solvent crystals is mostly based on physical interactions between them, which are the main formation mechanism of the porous structure. It is largely independent of the nature of the employed materials.[16] A large number of polymeric materials, such as chitin,[19] gelatin,[20] collagen,[21] poly(lactic acid),[22] poly(-lactic-*co*-glycolic acid),[23] agarose,[24] sericin,[25] and chitosan,[26] have been studied in the literature as proper materials for scaffold fabrication. Among the aforementioned materials, chitosan is a familiar, biodegradable polysaccharide that has properties that include biocompatibility, antibacterial activity, bioadhesivity, and wound healing.[26,27] Wide types of chitosan can be produced by changes in the deacetylation degree of chitin, which can be found as a subproduct of shellfish, such as crabs and shrimp.[28,29] The structural similarity of this polymer to natural glycosaminoglycans makes it superbiocompatible.[30] These

© 2014 Wiley Periodicals, Inc.

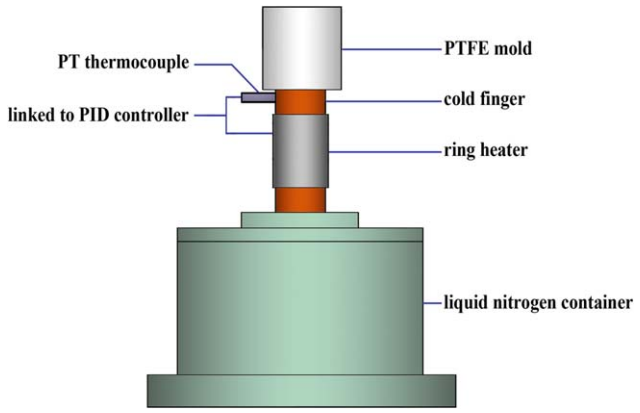

Figure 1. Schematic illustration of the freeze-casting setup used for the fabrication of the chitosan scaffolds. PT = platinum. [Color figure can be viewed in the online issue, which is available at www.wileyonlinelibrary.com.]

features have led to the use of chitosan in several implantable and injectable systems, such as orthopedic/periodontal composites,[31] drug-delivery systems,[32] wound-healing control,[33] and scaffolds for soft and hard tissue reconstruction.[34–36] Interesting processes have been undertaken to construct porous chitosan scaffolds with promising results, but an inherent lack of strength is still a common limitation.[37]

A freeze-casting method for the fabrication of chitosan scaffolds has not been used yet. In this study, we aimed to control the amount of solid concentration and freezing rate in a proper fashion to obtain a chitosan scaffold with a unidirectional structure and high compressive strength (σ) values.

EXPERIMENTAL

Preparation of the Scaffolds

The chitosan (Sigma Aldrich, 448877, Germany) used in this study had a medium molecular weight of about 190–310 kDa, a deacetylation degree of 75–85%, and a viscosity of 200–800 cps. Scaffolds were prepared by the freeze-casting method. At first, chitosan solutions with concentrations of 1.5 and 3 wt % were prepared by the dissolution of chitosan in deionized water with 2% acetic acid by volume (Merck, KGaA, 64271, Darmstadt, Germany) at 50°C with stirring for 1 day. Then, the prepared solution was poured into a polytetrafluoroethylene (PTFE) mold with an inner diameter of 20 mm. This mold was placed on a copper cold finger, where the temperature was controlled with liquid nitrogen and a ring heater connected to a proportional integral derivative (PID) controller, and the temperature was monitored by a thermocouple located near the surface of the cold finger. A schematic illustration of the device used for fabricating chitosan scaffolds is shown in Figure 1. The cooling rates applied in this study were 1 and 4°C/min. After very careful removal of the frozen samples from the mold, the samples were dried in a freeze dryer (FD-10, Pishtaz Engineering Co., Tehran, Iran) at a low temperature of −55°C and a pressure of 2.1 Pa for 48 h to sublimate ice crystals *in vacuo*. Finally, all of the samples were neutralized with 0.1*N* NaOH for 1 h. Then, excess base agents were removed by repeated washing with 40% ethanol and deionized water until the pH returned to the physiological range[38] and then freeze-dried again. The prepared samples were maintained in a silica gel desiccator for further characterization. The specifications of the samples are detailed in Table I.

Table I. Specifications of the Samples

Sample	Chi1.5R1	Chi1.5R4	Chi3R1	Chi3R4[a]
Chitosan (g/100 mL)	1.5	1.5	3	3
Cooling rate (°C/min)	1	4	1	4
Acetic acid (mL/100 mL)	1	1	2	2

[a] Chi3R4 is indicative of 3 wt % chitosan with cooling rate of 4°C/min.

Scanning Electron Microscopy (SEM) Analyses

The morphology and microstructure of the scaffolds were studied with an SEM (Stereoscan S 360-Leica, Cambridge, England) instrument. A thin layer of gold was coated over the surface of the prepared scaffolds to eliminate the poor conductivity of the sample's current before testing.

Porosity and Pore Size Evaluation

The porosity value of chitosan scaffolds, which depended on the chitosan concentration, was calculated by following formula:

$$\begin{aligned} \text{Porosity} &= (V_m - V_p)/V_m \times 100\% \\ &= [V_m - (W_m/\rho)]/V_m \times 100\% \end{aligned} \quad (1)$$

whereby V_m is the total volume of the chitosan scaffold (cm^3), V_p is the actual volume taken by chitosan (cm^3), W_m is the mass of the scaffold (g), and ρ is the density of chitosan measured by an automatic density analyzer (Micrometrics, AccuPyc 1330 Pycnometer) with an amount of 1.4499 ± 0.0083 (g/cm^3). The average pore channel size was determined by KLONK image measurement software. Ten lines, including four vertical lines, four horizontal lines, and two diagonal lines, were drawn on the SEM images taken from the axes perpendicular to the ice crystal growth direction. Then, the length of each line was divided into the number of pores that were cut by each line, and finally, the average pore channel size was measured.

Mechanical Behavior

The mechanical behavior of the prepared scaffolds was investigated by a compression strength test (SANTAM Engineering Design. Co., Tehran, Iran). The cylindrical samples, with a diameter of about 20 mm and a height of about 20 mm, were tested with a 100-kN load cell at crosshead speed of 0.5 mm/min. The compressive modulus (E) was calculated through the slope of the initial linear portion of the stress–strain curves. The maximum height of the curves after the initial linear portion was considered as σ. At least five samples were used to obtained reliable data.

Water Uptake

We calculated the uptake capacity of the chitosan scaffolds by submerging the samples in deionized water at 25°C. After they were kept in water for almost 2 h (+/− 5 min), the samples were carefully taken out. The surface of the samples was dried

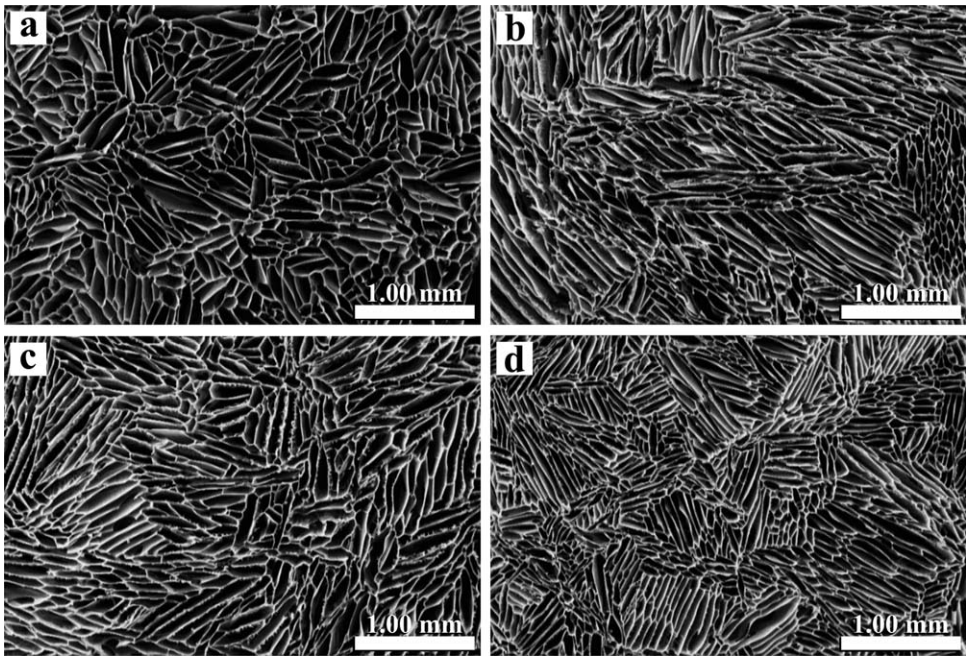

Figure 2. Effects of the changes in the chitosan concentration and the cooling rate on the pore structure of (a) Chi1.5R1, (b) Chi1.5R4, (c) Chi3R1, and (d) Chi3R4. The cross section was perpendicular to the ice growth front.

by filter papers, and the samples were weighed afterward. The water absorption was calculated with the following formula:

$$\text{Water absorption} = (w - w_0)/w_0 \times 100\% \quad (2)$$

whereby w_0 and w are weights of the scaffold before and after the water absorption test, respectively. All of the reported data mentioned previously were the mean values of five independent measurements.

RESULTS AND DISCUSSION

Morphology of the Chitosan Scaffolds

The pore morphology and microstructure of the scaffolds were observed with SEM images. A directional structure was fashioned by the application of a thermal gradient on the chitosan scaffolds solutions in a freeze-casting technique. The thermal gradient took place because of a large difference between the thermal conductivity of the copper mold, which was cooled with liquid nitrogen during the freezing process, and the PTFE mold. The existence of this strong thermal gradient led to the transmission of the solution's heat downward to the copper mold; this guided the growth of ice crystals in the reverse direction. As ice crystals grew upward, the chitosan molecules floating in the solution were repelled from tip of the ice crystals and became packed between them. Finally, after the freeze-drying process was applied on the freeze-cast scaffolds to evaporate their ice crystals, lamellar structures were formed.[12] Figure 2 illustrates the effect of the changes in the chitosan concentration and cooling rate on the perpendicular direction of ice growth. As it shows, at constant concentrations of chitosan, both 1.5 and 3 wt %, an increase in the cooling rate from 1 to 4°C/min resulted in a decrease in the pores size, and this was because of the contrast between the nucleation and growth mechanisms during the process of freezing. Because of the formation of more ice nucleation and less time for growth in high cooling rates, the nucleation process preceded the growth process.[12] Thus, the final structure of the scaffold included more lamella of thin ice walls, and this resulted in more pores with smaller size. Also, at constant cooling rates, both 1 and 4°C/min, an increase in the chitosan concentration from 1.5 to 3 wt % augmented the viscosity of solution, and under these conditions, the pushing of the chitosan molecules away from the solidification front was difficult, and this led to a limitation of the ice growth mechanism. Consequently, the ice crystals were thinner than in the previous state, and this resulted in a smaller pore size and thicker chitosan walls.[20] The average pore channel size values of each chitosan scaffold were measured, and they are reported in Table II. In addition, Figure 3 shows SEM images taken from the parallel direction of ice growth; this illustrates the appearance of pores in the chitosan walls, which resulted in more interconnectivity in the body of the scaffold. It seemed that a low surface tension of the chitosan walls led to the penetration and growth of some ice crystals in the perpendicular direction of ice growth and the piercing of the thin chitosan walls. As a result, the ice lamellae made a cross contact together and created interconnect pores in the

Table II. Porosity and Average Pore Channel Size Measurements of the Chitosan Scaffolds

Sample name	Chi1.5R1	Chi1.5R4	Chi3R1	Chi3R4
Porosity (%)	98.36 ± 0.043	98.19 ± 0.092	96.60 ± 0.052	96.43 ± 0.062
Average pore channel size (μm)	99.7 ± 0.53	89.1 ± 0.81	75.0 ± 0.83	58.8 ± 0.48

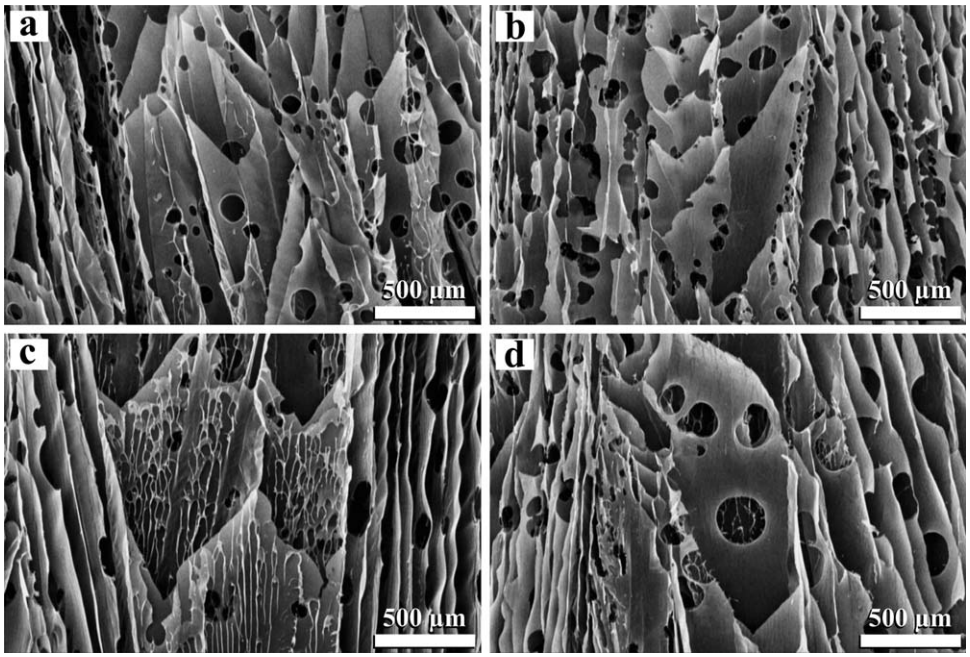

Figure 3. Effects of the changes in the chitosan concentration and cooling rate on the pore structure of (a) Chi1.5R1, (b) Chi1.5R4, (c) Chi3R1, and (d) Chi3R4. The cross section was parallel to the ice growth front.

chitosan scaffold.[39] In addition, as shown in Figure 3, at constant concentrations, an increase in the cooling rate raised the number of pores in the chitosan walls. It seemed that an increase in number of walls and, therefore, the state of having less thickness in the high cooling rate condition resulted in a reduction of the wall resistance toward piercing. Also, at constant cooling rates, with an increase in the chitosan concentration, the number of pores located in the walls decreased; this could have been due to an elevation in the thickness of the chitosan walls. Under these condition, it was more difficult for the ice crystals to penetrate and pierce the chitosan walls.

Porosity Measurements

The porosity and pore size are important morphological properties of biomaterial scaffolds for the regeneration of tissues.[40] The numerical measurements of porosity and average pore channel size for each chitosan scaffold that was prepared by the freeze-casting method was measured, and these values are reported in Table II. With regard to the porosity values, changes in the freezing rate did not have a sizeable effect on the porosity amount, but an increase in the chitosan concentration resulted in a decrease in the scaffold's porosity. This phenomenon occurred because more of the occupying materials were at a constant volume; this intensified the actual volume fraction, and this led to a reduction in the porosity and made the scaffolds stronger.[16,18]

In addition, it is worth mentioning that the formation of colonies (the space that included approximately the same pores in the case of size and parallel chitosan walls) in the samples, which were constructed at a cooling rate of 4°C/min, is noticeable. Figure 4 depicts the SEM images of chitosan scaffolds that were fabricated at a freezing rate of 4°C/min. As the figure shows, in these samples, in comparison to those in Figure 2(a,c), which were fabricated at a freezing rate of 1°C/min, there were two types of pores with small and large sizes, which made colonies with greater size. Also, the colonies formed in sample Chi1.5R4 were larger than the colonies formed in sample Chi3R4. In general, porous scaffolds with small pores have

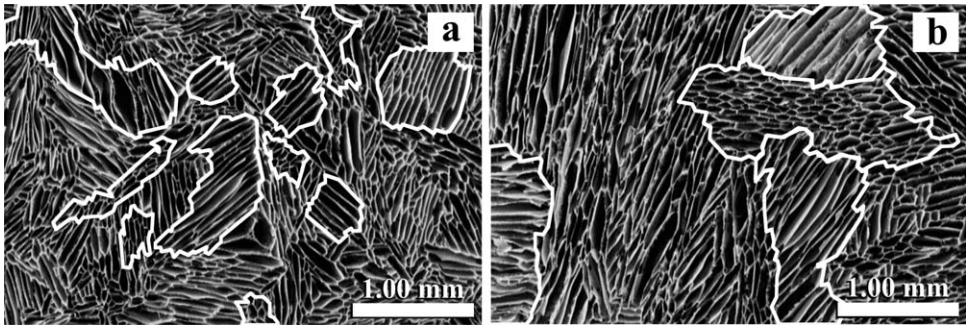

Figure 4. SEM images of samples (a) Chi3R4 and (b) Chi1.5R4, which illustrate the colonies of pores that included approximately the same pore size associated with parallel chitosan walls.

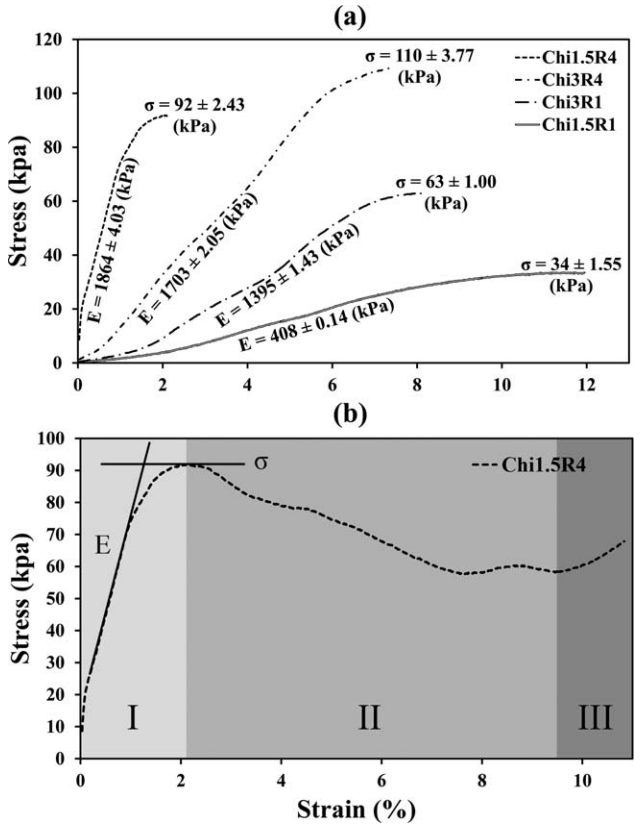

Figure 5. (a) Compression stress–strain curves of the chitosan scaffolds with different concentrations and freezing rates along with the σ value and E value. (b) Complete stress–strain curve of sample Chi1.5R4, which shows three discrete slope regions.

advantages such as a great σ, which is necessary for regeneration in load-bearing tissues,[41] and a large surface area, which leads to better cell attachment.[42] Also, scaffolds with large pores have a more favorable structure for cell generation and the facilitation of tissue regeneration. Therefore, scaffolds with both fine and large pores have great advantages compared to scaffolds with just small or just large pores.

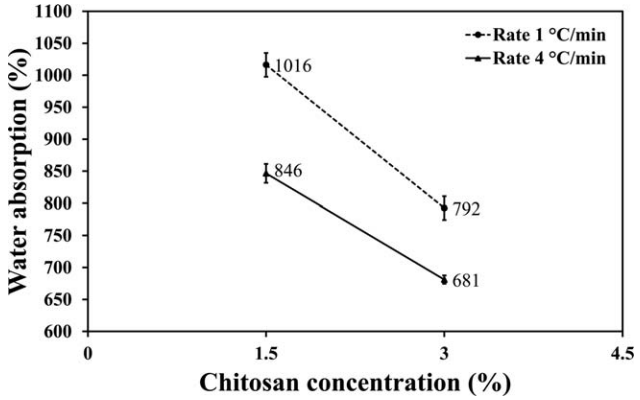

Figure 6. Water absorption behaviors of the chitosan scaffolds fabricated with different chitosan concentrations and freezing rates.

Mechanical Behavior

To support tissue regeneration at the site of implantation and sustain sufficient integrity during both *in vitro* and *in vivo* cell growth, scaffolds need to have enough mechanical strength for these purposes.[43,44] As the ice-template freeze-casting results in a unidirectional and inhomogeneous structure, the parallel and vertical direction during casting will produce different mechanical strengths. In this study, to measure the σ values of the scaffolds, a compressive load was applied in the direction parallel to the growth of ice crystals. Figure 5(a) shows the compression stress–strain curves of the chitosan scaffolds with different concentrations and freezing rates along with the σ and E value for each one. As shown, at constant concentrations, with an increase in the cooling rate from 1 to 4°C/min, σ improved. This was due to both a reduction in pore size and an increase in the number of chitosan walls that bore the compressive load according to the previous discussion. Moreover, at constant freezing rates, σ was augmented by an increase in the chitosan concentration from 1.5 to 3 wt %; this was attributed to a decrease in the pore size and porosity and also an increase in the thickness of the chitosan walls. In the case of the modulus, the effect of an increase in the cooling rate on E in the samples with 1.5 wt % chitosan was larger than that of the samples with 3 wt %. This might have been linked to the larger colonies of pores in sample Chi1.5R4 compared to those in sample Chi3R4; this created a structural homogeneity[45] of the parallel chitosan walls, shown in Figure 4. This structural homogeneity of parallel chitosan walls potentially resulted in a more equal load transfer across the sample upon compressive testing. In summary, σ and E ranges of the ice-templated scaffolds were 34 to 110 kPa and 408 to 1864 kPa, respectively. According to the literature, the σ of pure porous chitosan scaffolds with a concentration of about 2 wt % is generally low around 30 kPa, with a reported modulus value of around 346 kPa; this was lower than what we achieved.[45–47] In connection with Figure 5(b), the complete curve of sample Chi1.5R4 was chosen to explain more about the mechanical behavior of the scaffolds during the σ test. As this depicts, there were three discrete regions. Region I was a linear elastic regime caused by internal pore bending. Region II was a collapse plateau regime, which was caused by pore buckling or collapse. Region III was a densification regime; this was due to complete pore collapse throughout the scaffold.[48] In general, the balance between the adequate material porosity and mechanical strength was one of the main challenges in the fabrication of the porous scaffolds.[44] The previous results show that this balance improved because of the unidirectional pores and homogeneous structure of the scaffolds fabricated by the ice-templating method.

Water Uptake

The water-binding ability of the scaffolds was attributed to the hydrophilic nature of the chitosan, scaffold pores size, and their spatial interconnectivity.[35] The water absorption behavior of the chitosan scaffolds fabricated by different chitosan concentrations and freezing rates are shown in Figure 6. As mentioned previously, with increasing chitosan concentration, the pores size and porosity of the scaffolds decreased. Therefore, a decrease in the amount of water absorbed seemed reasonable. Numerical

measurements showed that when the chitosan concentration changed from 3 to 1.5 wt %, the absorption values elevated by approximately 1.26 times. Also, an increase in the cooling rate at a constant concentration influenced the water absorption because of the reduction of the pore size, and this slightly impeded the absorption mechanism. The immersion of the scaffold in water increased the pore size, and this provided a better supplement of nutrients and oxygen in the interior regions, but a lack of strength in the scaffold and a high rate of degradation are some of the drawbacks that should be considered further.[49]

CONCLUSIONS

In this article, we have reported the potential of using different freezing rates and chitosan concentrations during a freeze-casting method to investigate the characteristics of chitosan scaffolds with unidirectionally aligned pore channels containing pore walls for biomaterial applications. Increases in the freezing rate and chitosan concentration had the same effects on the pore channel size and water absorption and reduced both of them. The porosity did not change, although the freezing rate decreased, but a reduction in the chitosan concentration led to an increase in the porosity. σ also improved with augmentations of the chitosan concentration and cooling rate. In addition, an increase in the cooling rate had a great effect on the elevation of the modulus at a 1.5 wt % chitosan concentration; this was attributed to the formation of large colonies of pores.

REFERENCES

1. Garrido, L. B.; Albano, M. P.; Plucknett, K. P.; Genova, L. *J. Mater. Process. Technol.* **2009**, *209*, 590.
2. Ravichandran, K. S.; An, K.; Dutton, R. E.; Semiatin, S. L. *J. Am. Ceram. Soc.* **1999**, *82*, 673.
3. Hong, C.; Zhang, X.; Han, J.; Du, J.; Han, W. *Scr. Mater.* **2009**, *60*, 563.
4. Li, Z.; Ramay, H. R.; Hauch, K. D.; Xiao, D.; Zhang, M. *Biomaterials* **2005**, *26*, 3919.
5. Gutiérrez, M. C.; Ferrer, M. L.; del Monte, F. *Chem. Mater.* **2008**, *20*, 634.
6. Pandey, S.; Mishra, S. B. *J. Colloid Interface Sci.* **2011**, *361*, 509.
7. Kong, D.; Yang, H.; Wei, S.; Li, D.; Wang,; *J. Ceram. Int.* **2007**, *33*, 133.
8. Ji, C.; Annabi, N.; Khademhosseini, A.; Dehghani, F. *Acta Biomater.* **2011**, *7*, 1653.
9. Zhao, J.; Han, W.; Chen, H.; Tu, M.; Zeng, R.; Shi, Y.; Cha, Z.; Zhou, C. *Carbohydr. Polym.* **2011**, *83*, 1541.
10. Elsabee, M. Z.; Naguib, H. F.; Morsi, R. E. *Mater. Sci. Eng. C* **2012**, *32*, 1711.
11. Kim, M. Y.; Lee,; *J. Carbohydr. Polym.* **2011**, *84*, 1329.
12. Li, W. L.; Lu, K.; Walz, J. Y. *Int. Mater. Rev.* **2012**, *57*, 37.
13. Colard, C. A. L.; Cave, R. A.; Grossiord, N.; Covington, J. A.; Bon, S. A. F. *Adv. Mater.* **2009**, *21*, 2894.
14. Han, J.; Hong, C.; Zhang, X.; Du, J.; Zhang, W. *J. Eur. Ceram. Soc.* **2010**, *30*, 53.
15. Yook, S.-W.; Kim, H.-E.; Koh, Y.-H. *Mater. Lett.* **2009**, *63*, 1502.
16. Deville, S. *Materials* **2010**, *3*, 1913.
17. Hong, C.; Zhang, X.; Han, J.; Du, J.; Zhang, W. *Mater. Chem. Phys.* **2010**, *119*, 359.
18. Deville, S. *Adv. Eng. Mater.* **2008**, *10*, 155.
19. Madihally, S. V.; Matthew, H. W. *Biomaterials* **1999**, *20*, 1133.
20. Arabi, N.; Zamanian, A. *Biotechnol. Appl. Biochem.* **2013**, *60*, 573.
21. Schoof, H.; Bruns, L.; Fischer, A.; Heschel, I.; Rau, G. *J. Cryst. Growth* **2000**, *209*, 122.
22. Ho, M.-H.; Kuo, P.-Y.; Hsieh, H.-J.; Hsien, T.-Y.; Hou, L.-T.; Lai, J.-Y.; Wang, D.-M. *Biomaterials* **2004**, *25*, 129.
23. Maquet, V.; Boccaccini, A. R.; Pravata, L.; Notingher, I.; Jérôme, R. *Biomaterials* **2004**, *25*, 4185.
24. Stokols, S.; Tuszynski, M. H. *Biomaterials* **2004**, *25*, 5839.
25. Tao, W.; Li, M.; Xie, R. *Macromol. Mater. Eng.* **2005**, *290*, 188.
26. Di Martino, A.; Sittinger, M.; Risbud, M. V. *Biomaterials* **2005**, *26*, 5983.
27. Kim, I.-Y.; Seo, S.-J.; Moon, H.-S.; Yoo, M.-K.; Park, I.-Y.; Kim, B.-C.; Cho, C.-S. *Biotechnol. Adv.* **2008**, *26*, 1.
28. Chenite, A.; Chaput, C.; Wang, D.; Combes, C.; Buschmann, M.; Hoemann, C.; Leroux, J.; Atkinson, B.; Binette, F.; Selmani, A. *Biomaterials* **2000**, *21*, 2155.
29. Kas, H. S. *J. Microencapsulation* **1997**, *14*, 689.
30. VandeVord, P. J.; Matthew, H. W.; DeSilva, S. P.; Mayton, L.; Wu, B.; Wooley, P. H. *J. Biomed. Mater. Res.* **2002**, *59*, 585.
31. Khor, E.; Lim, L. Y. *Biomaterials* **2003**, *24*, 2339.
32. Ruel-Gariépy, E.; Chenite, A.; Chaput, C.; Guirguis, S.; Leroux, J. C. *Int. J. Pharm.* **2000**, *203*, 89.
33. Keshun, L. Soybeans: Chemistry, Technology, and Utilization; Chapman & Hall: New York, **1997**.
34. Ho, M.-H.; Wang, D.-M.; Hsieh, H.-J.; Liu, H.-C.; Hsien, T.-Y.; Lai, J.-Y.; Hou, L.-T. *Biomaterials* **2005**, *26*, 3197.
35. Ma, L.; Gao, C.; Mao, Z.; Zhou, J.; Shen, J.; Hu, X.; Han, C. *Biomaterials* **2003**, *24*, 4833.
36. Muzzarelli, R.; Mattioli-Belmonte, M.; Tietz, C.; Biagini, R.; Ferioli, G.; Brunelli, M.; Fini, M.; Giardino, R.; Ilari, P.; Biagini, G. *Biomaterials* **1994**, *15*, 1075.
37. Deville, S.; Saiz, E.; Tomsia, A. P. *Biomaterials* **2006**, *27*, 5480.
38. Zhu, Y.; Liu, T.; Song, K.; Jiang, B.; Ma, X.; Cui, Z. *J. Mater. Sci. Mater. Med.* **2009**, *20*, 799.
39. Geng, X.; Kwon, O.-H.; Jang,; *J. Biomaterials* **2005**, *26*, 5427.
40. Hutmacher, D. W. *Biomaterials* **2000**, *21*, 2529.
41. Karageorgiou, V.; Kaplan, D. *Biomaterials* **2005**, *26*, 5474.

42. O'Brien, F. J.; Harley, B. A.; Yannas, I. V.; Gibson, L. *J. Biomaterials* **2005**, *26*, 433.

43. Chu, T. M. G.; Orton, D. G.; Hollister, S. J.; Feinberg, S. E.; Halloran, J. W. *Biomaterials* **2002**, *23*, 1283.

44. Thomson, R. C.; Yaszemski, M. J.; Powers, J. M.; Mikos, A. G. *J. Biomater. Sci. Polym. Ed.* **1996**, *7*, 23.

45. Liu, M.; Wu, C.; Jiao, Y.; Xiong, S.; Zhou, C. *J. Mater. Chem. B* **2013**, *1*, 2078.

46. Sweetman, L. J.; Moulton, S. E.; Wallace, G. G. *J. Mater. Chem.* **2008**, *18*, 5417.

47. Zhao, L.; Chang, J. *J. Mater. Sci. Mater. Med.* **2004**, *15*, 625.

48. Harley, B. A.; Leung, J. H.; Silva, E. C. C. M.; Gibson, L. *J. Acta Biomater.* **2007**, *3*, 463.

49. Peter, M.; Binulal, N. S.; Soumya, S.; Nair, S. V.; Furuike, T.; Tamura, H.; Jayakumar, R. *Carbohydr. Polym.* **2010**, *79*, 284.